ISSN 1392-2114 ULTRAGARSAS (ULTRASOUND), Vol. 66, No. 2, 2011.

A viscoelastic plate theory for the fast modelling of Lamb wave solutions in NDT/SHM applications

M. A. Torres-Arredondo [1,2], C.-P. Fritzen [1,2]

[1] *University of Siegen, Centre for Sensor Systems; Siegen, Germany*

[2] *University of Siegen,. Institute of Mechanics and Control Engineering-Mechatronics; Siegen, Germany*

Phone: +49 271 7402132, Fax: +49 271 7402769; e-mail: {torres, fritzen}@imr.mb.uni-siegen.de

crossref http://dx.doi.org/10.5755/j01.u.66.2.524

Abstract

Guided ultrasonic waves have many useful properties that can be exploited for non-destructive testing (NDT) and structural health monitoring (SHM) applications. However, much information and analysis regarding the generation and propagation of these waves is needed before automatic processing and analysis techniques can provide useful information for reliable fault monitoring. Moreover, the knowledge of dispersion characteristics is crucial for the optimization of sensor networks in terms of sensor placement and number of sensors. On that account, the present work introduces a higher order plate theory for modelling disperse solutions in viscoelastic fibre-reinforced composites. This approach offers a higher computational efficiency and simplicity in comparison to traditional exact elasticity methods, while providing an adequate description of the structure's global response in the low frequency range which is the most used in Lamb wave applications. The proposed method was applied to several examples in order to obtain numerical results in elastic and viscoelastic anisotropic plates. Some comparisons to experimental data are presented, and the effectives and limitations of the method are discussed.

Keywords: Lamb waves, plate theory, viscoelasticity, fibre composite, structural health monitoring

1. Introduction

Guided ultrasonic waves are a valuable tool in order to get information regarding the origin and importance of a discontinuity in a structure for a longer safe life and lower operation costs [1]. Depending on the material attenuation and geometric beam spreading effects, guided waves are able to propagate over relative long distances, interact sensitively with and/or being related to different types of defects like e.g. delaminations, corrosion damage, etc. However, it is only possible to benefit from these advantages once the complexity of guided wave propagation are disclosed. Generally, there are two ways to obtain such complex dispersion characteristics. The first strategy is based on common experimental time-delay measurements where piezoelectric transducers are attached to a structure and play the role of either actuator or sensor. A second approach is based on different modelling approaches, where material constants are measured by means of different identification or material testing techniques and then fed into an analytic or finite element model to extract the relevant information. The situation considered in this paper is representative of the latter case.

The modelling of wave propagation in multilayered anisotropic structures has been extensively studied by several researchers and a considerable amount of literature has been published on this topic [2]. Analyzing guided waves in these structures is often categorized into three methods. There are methods based on exact three dimensional elasticity, waveguide finite element methods and laminated plate theories of different orders. Exact methods are based on the superposition of bulk waves that include the popular matrix based methods [3]. Waveguide finite element methods have appeared for modelling the guided wave propagation numerically as an alternative to exact methods by using a finite element discretization of the cross-section of the waveguide [4]. A different alternative providing simplicity and low computational cost in comparison to other techniques are laminated plate theories. These theories expand the displacement fields in terms of the thickness to any desired degree and reduced the 3-D continuum problem to a 2-D problem. There are many papers dealing with plate theories and their applications; some notable work in this field is given by Reddy in [5]. The present work proposes a third order plate theory that can approximate five symmetric and six antisymmetric Lamb wave modes. Here, the two classical models of viscoelastic attenuation are implemented and discussed. Previous related work to the one proposed here using a second order expansion of the displacement fields in terms of the thickness was presented by Calomfirescu in [6]. However, this work was restricted to the analysis of just the fundamental modes of propagation and the use of one model of attenuation for computational reasons. The motivation for expanding the displacement field up to the cubic term in the thickness is to provide better kinematics and accurate interlaminar stress distributions [7]. Moreover, the complex root finding algorithms needed with the exact methods are not required here since analytical solutions can be obtained and reduce to the solution of simple polynomials. Since the use of composite materials has extensively increased in the design of existing engineering structures, what also increases the analysis complexity of such structures, this poses a necessity for fast modelling tools that can be used for a rapid and reliable analysis.

2. Material damping models for wave propagation

The mathematical modeling of viscoelasticity using ideas from elasticity has attracted the attention of a large number of investigators over the past century. In order to account for material damping, the stiffness matrix is represented by a complex quantity. The real part C of this

complex term relates to the elastic behaviour of the material and defines the stiffness. The imaginary component η relates to the material viscous behaviour and defines the energy dissipative ability of the material. Two models are often used to describe viscoelastic behaviour. The first model is called the hysteretic model whose complex stiffness matrix is given by

$$\widetilde{C} = C + i\eta\,. \tag{1}$$

The hysteretic model assumes no frequency dependence of the viscoelastic constants. The second model is the Kelvin-Voigt model and assumes a linear dependence of the viscoelastic coefficients. The complex stiffness matrix is expressed as

$$\widetilde{C} = C + i\frac{\omega}{\widetilde{\omega}}\eta\,, \tag{2}$$

where ω is the angular frequency and $\widetilde{\omega}$ is the frequency of characterization. The influence in the attenuation predicted by both methods for the fundamental modes of propagation is depicted in Fig. 1. The characterization frequency is 2 MHz.

From the previous picture it can be clearly seen that the attenuation is a linear function of the frequency in the case of the hysteretic model and a quadratic function of the frequency in the case of the Kelvin–Voigt model. Additionally, both models are just coincident in the frequency of characterization and away from this point, the deviation in the prediction of both models is noteworthy.

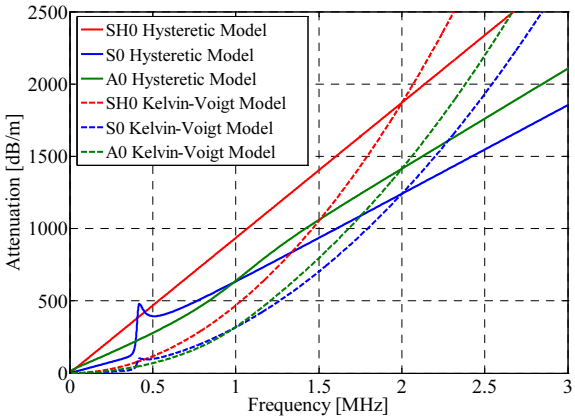

Fig. 1. **Comparison of attenuation between the hysteretic and Kelvin-Voigt models as a function of frequency**.

3. Mathematical framework for the plate theory

The model considers a linearly viscoelastic, non-piezoelectric layer of material subjected to a complex stress system in three dimensions. The material is considered to have a monoclinic symmetry. Fig. 2 depicts the definition of stress resultants (N, M, Q) in the three dimensional system for a given propagation direction θ and fiber orientation φ.

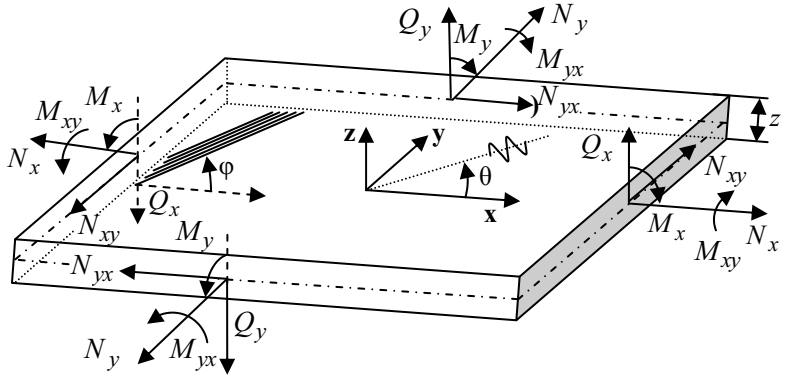

Fig. 2. **Complex stress system in three dimensions**

The approximated displacement fields are given by

$$\begin{aligned} u &= u_0(x,y,t) + z\psi_x(x,y,t) + z^2\phi_x(x,y,t) + z^3\lambda_x(x,y,t) \\ v &= v_0(x,y,t) + z\psi_y(x,y,t) + z^2\phi_y(x,y,t) + z^3\lambda_y(x,y,t) \\ w &= w_0(x,y,t) + z\psi_z(x,y,t) + z^2\phi_z(x,y,t), \end{aligned} \tag{3}$$

where u, v, and w are the displacement components in x, y and z directions, θ_x and θ_y represent rotations having the same meaning as in the first order shear deformation theory [8]. The additional terms expand the displacement field. The strain energy of each layer can be represented as [9]

$$U = \frac{1}{2}\int_V \begin{pmatrix} C_{11}\varepsilon_x^2 + 2C_{12}\varepsilon_x\varepsilon_y + 2C_{13}\varepsilon_x\varepsilon_z + 2C_{16}\varepsilon_x\gamma_{xy} + \\ + C_{22}\varepsilon_y^2 + 2C_{23}\varepsilon_y\varepsilon_z + 2C_{26}\varepsilon_y\gamma_{xy} + C_{33}\varepsilon_z^2 + \\ + 2C_{36}\varepsilon_z\gamma_{xy} + C_{66}\gamma_{xy}^2 + C_{44}\gamma_{yz}^2 + \\ + 2C_{45}\gamma_{yz}\gamma_{xz} + C_{55}\gamma_{xz}^2 \end{pmatrix} dV. \tag{4}$$

Additionally,

$$\sigma_x = \frac{\partial U}{\partial \varepsilon_x}, \ldots, \tau_{xy} = \frac{\partial U}{\partial \gamma_{xy}}\,. \tag{5}$$

The plate constitutive equations may be derived from the strain energy density in the 3-D elasticity theory and the linear elastic stress-strain and strain-displacement

relations. The equations of motion may be derived from the dynamic version of the principle of virtual displacement. Consequently, the system can be expressed in a matrix form, and by imposing boundary conditions and setting its determinant to zero, a characteristic function relating the angular frequency to the wavenumber is obtained. For the case of symmetric laminates, the system of equations can be decoupled into two independent systems of equations for the symmetric and antisymmetric modes of propagation. A comparison between exact solutions and a similar elastic third order plate theory is provided by Wang and Yuan in [10]. However, this paper does not document the relevant results needed for the calculation of the dispersion relations and uses different shear correction factors to the ones provided here. A complete description of the numerical strategy for the tracing of the dispersion solutions is presented in [11]. The complete analytical expressions are given in the appendix of this paper.

4. Results

The proposed viscoelastic plate theory formulation is applied to several examples including two anisotropic elastic plates and two anisotropic viscoelastic plates.

4.1. Elastic glass fibre reinforced plastic plate

In order to validate the modelling approach, a case study has been conducted on a unidirectional glass-fibre reinforced plastic (GFRP) plate. A single-layered specimen was selected because of its highly anisotropic character. Fig. 3a shows the structure that has the dimensions 800 mm×800 mm and a thickness of approximately 1.5 mm. Nine piezoelectric transducers are attached to the surface of the structure with equidistant spacing. The piezo patches have a diameter of 10mm and a thickness of 0.25 mm. The elastic properties in the principal directions of material symmetry provided by the manufacturer are given in Table 1.

The experimental group velocities were determined in the defined frequency by means of time-delay measurements. Numerical results for the group velocities for the fundamental modes of propagation at a central frequency of 200 kHz are depicted in Fig. 3b. The wave surface for the S_0 mode at 200 kHz is shown in comparison with some measured values at discrete angular points (black circles) in order to validate the analytical model with experimental data. It can be seen that the estimated group velocity matches the theoretical curve very well, demonstrating the effectiveness of the model.

Table 1. **Material properties of unidirectional glass fibre reinforced plastic**

E_1 (GPa)	E_2 (GPa)	E_3 (GPa)	G_{12} (GPa)	G_{13} (GPa)	G_{23} (GPa)	υ_{12}= υ_{13}= υ_{23}	ρ (kg/m^3)
30.7	15.2	10	4	3.1	2.75	0.3	1700

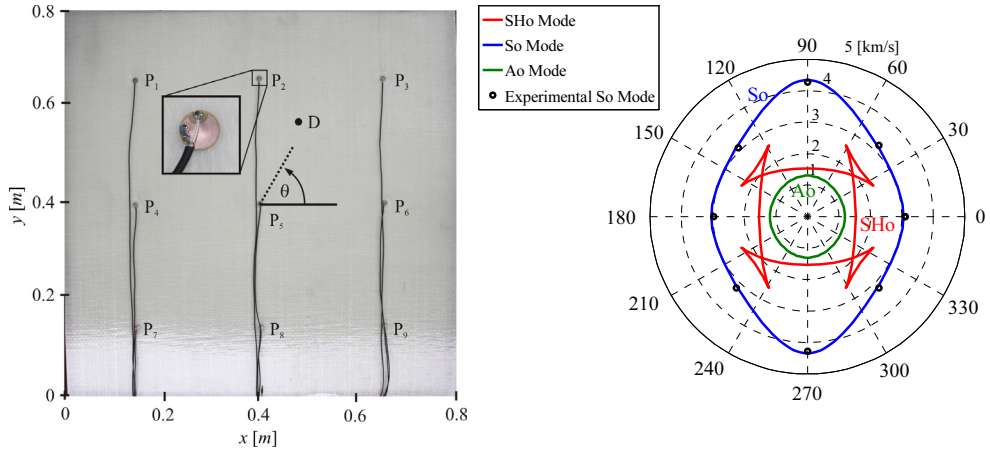

a b

Fig. 3. **Propagation modes: a - experimental setup, b - wave surface for the 1.5 mm thick GFRP in vacuum**

4.2. Elastic carbon fibre reinforced plastic plate

A carbon fibre reinforced plastic (CFRP) plate made of 16 equal layers is analyzed in this section. The stacking sequence is $[0\ 90\ -45\ 45\ 0\ 90\ -45\ 45]_s$ and the total thickness is 4.2 mm. The nominal material parameters of the unidirectional layers provided by the manufacturer are given in Table 2. Fig. 4a shows the plate of approximately 500 mm × 500 mm instrumented with nine piezoelectric transducers. A 3 cycle tone burst signal with a 60 kHz centre frequency was used as the input waveform. The piezoelectric transducer number five was designated as the actuator. Fig. 4b depicts the signals received by the sensors PZT4 and PZT2. In contrast to the previous GFRP plate, here it can be observed by checking the times of arrival and shapes of the received signals that the studied CFRP plate has an evident lower anisotropic behaviour (see also Fig. 4c). Furthermore, the fundamental antisymmetric mode is more strongly excited than that of the fundamental symmetric mode. The modes of propagation were identified by means of time-frequency analysis.

The calculated group velocities at θ=30° are depicted in Fig. 4d. It can be noticed that the behaviour of the SH_0 and S_0 modes is different from the A_0 mode in both the low and high frequency zones. In the relatively low frequency.

Table 2. **Material properties of multilayered carbon fibre reinforced plastic.**

E_1 (GPa)	E_2 (GPa)	E_3 (GPa)	G_{12} (GPa)	G_{13} (GPa)	G_{23} (GPa)	υ_{12}= υ_{13}= υ_{23}	ρ (kg/m^3)
155.0	8.5	8.5	4.0	4.0	4.0	0.33	1600

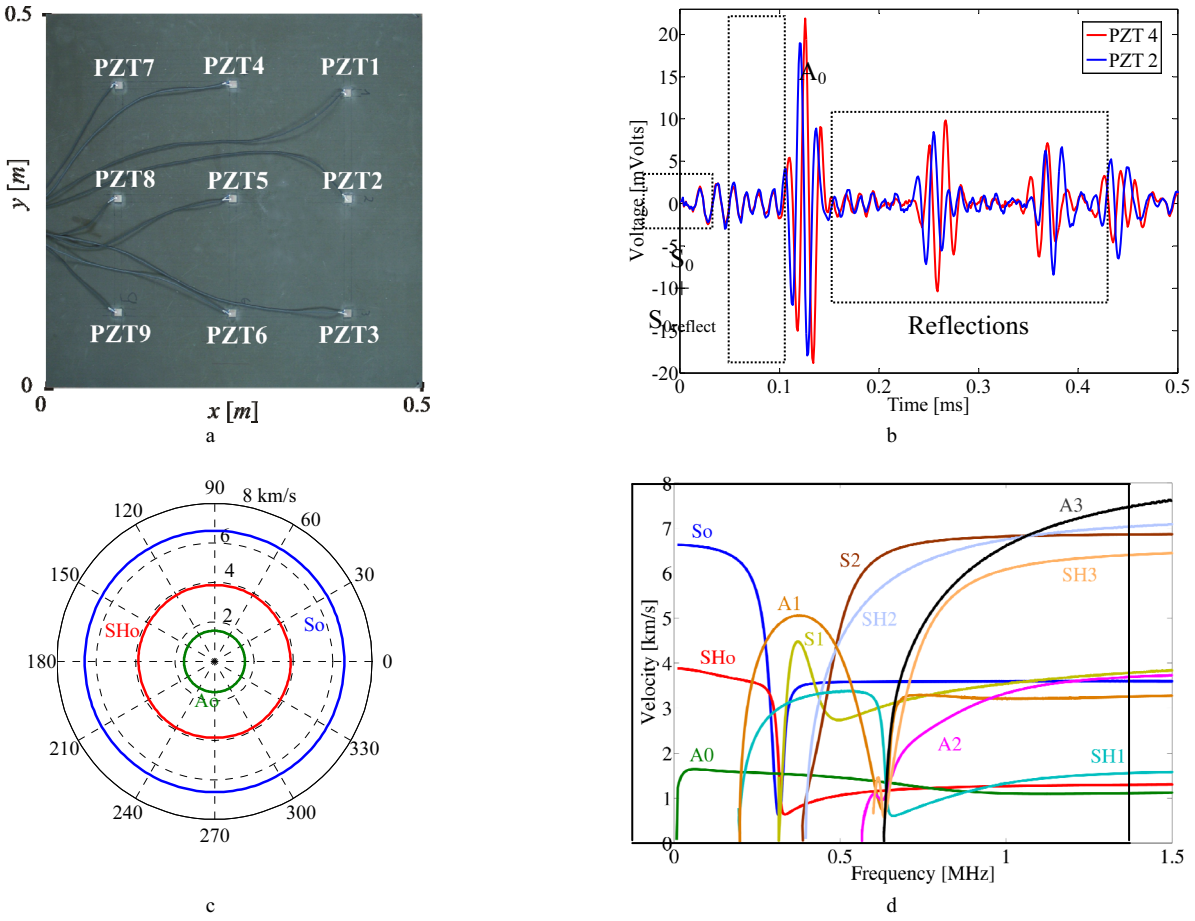

Fig. 4. **Propagation modes: a - experimental setup, b - recorded signals at the PZT sensors, c - wave surface at 60 kHz, d - group velocity dispersion curve**.

range the higher the frequency of the A_0 mode, the faster its group velocity. In an opposite manner for the S_0 mode, the higher its frequency, the slower its group velocity

4.3. Viscoelastic orthotropic carbon-epoxy plate

A viscoelastic orthotropic unidirectional lamina of 1mm of thickness is analyzed in this section. This example was fully studied in references [12-13]. The elastic and viscoelastic material properties are given in Table 3. The material was characterized at 2.242 MHz by the use of ultrasonic waves transmitted through a plate-shaped sample immersed in water.

Table 3. **Material properties of unidirectional carbon-epoxy 1 mm thick plate (units in GPa) [12]**

C_{11}	C_{12}	C_{13}	C_{22}	C_{23}	C_{33}	C_{44}	C_{55}	C_{66}
132	6.9	12.3	5.9	5.5	12.1	3.32	6.21	6.15
η_{11}	η_{12}	η_{13}	η_{22}	η_{23}	η_{33}	η_{44}	η_{55}	η_{66}
0.4	0.001	0.016	0.037	0.021	0.043	0.009	0.015	0.02

Fig. 5 presents the Lamb wave results obtained for both the hysteretic and the Kelvin-Voigt viscoelastic models. It can be clearly seen from Fig. 5a and b that both models do not affect the phase velocity results in a substantial manner. The results obtained with the proposed method are in good agreement with those obtained in references [12-13] for the A_0 and SH_0 fundamental modes of propagation. Although not depicted here (see [13]), the approximate solutions of S_0 mode have a good agreement with exact solutions at the lower frequency range, but a big divergence of the S_0 mode occurs at the zone of high dispersion around 1.5 MHz. For the higher order modes, solutions can be tracked very well at the beginning of zones of high dispersion; however, after these zones, results are not longer accurate and the higher order plate theory fails in providing good estimates for the velocities. Fig. 5a and b show that the effect in the prediction of attenuation for both models is appreciable when the working frequency is different from the characterization frequency.

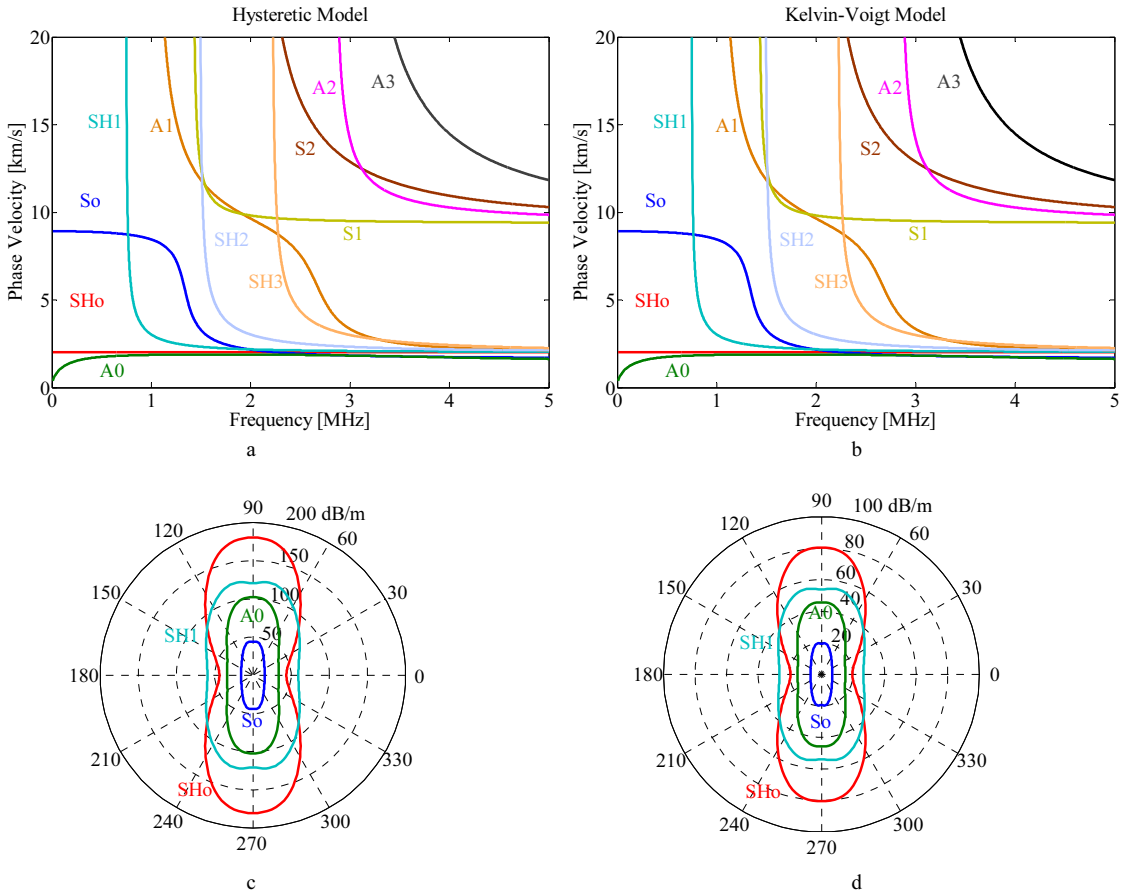

Fig. 5. **Comparison between the Hysteretic and Kevin-Voigt models: a - and b - phase velocity dispersion curves, c, d - attenuation polar plots at 500 MHz**.

4.4. Viscoelastic unidirectional carbon-epoxy plate

A viscoelastic unidirectional carbon-epoxy panel of 3.6 mm thickness is analyzed here. This example was chosen since it was fully studied by Neau in [14] by using a method based on the exact elasticity theory. The elastic and viscoelastic material properties are given in Table 4. The material was characterized at 2 MHz using conventional interferometry methods

Table 4. Material properties of unidirectional carbon-epoxy 3.6 mm thick plate (units in GPa) [14].

C_{11}	C_{12}	C_{13}	C_{22}	C_{23}	C_{33}	C_{44}	C_{55}	C_{66}
86.6	9	6.4	13.5	6.8	14	2.72	4.06	4.7
η_{11}	η_{12}	η_{13}	η_{22}	η_{23}	η_{33}	η_{44}	η_{55}	η_{66}
7.5	0.3	0.6	0.6	0.25	0.28	0.1	0.12	0.28

Fig. 6 depicts the attenuation of Lamb modes in polar coordinates for the 3.6 mm thick carbon-epoxy plate. The hysteretic model was used for this numerical example. Although not depicted here, the results obtained with the proposed method (Fig. 6a and b) are coincident with those obtained by Neau in [14] for the fundamental modes of propagation at 100 kHz. However, as one moves along the frequency axis to higher frequencies, i.e. 500 kHz , the predictions for the symmetric modes of propagation start to highly deviate from the exact solutions (Fig. 6c and Ref. [14]). Nevertheless, the good accuracy for the antisymmetric modes of propagation still holds for this frequency (Fig. 6d). This can be explained by the fact that the displacement field for the flexural motion is one order higher than that of the extensional motion, what assures a better approximation of the flexural modes. It can also be seen that the mode attenuation is strongly related to the frequency and orientation of propagation. This is a common characteristic of anisotropic materials where the velocity, attenuation and energy of propagation of the multiple modes are both frequency and angle dependent.

5. Discussion and conclusions

A coupling between viscoelasticity theory and a laminated plate theory has been suggested which is applicable to viscoelastic fibre reinforced composite materials for the calculation of wave velocities and attenuation for the different modes of propagation. The proposed theory poses a compromise between low computational cost and accuracy in the results. It has been shown that the method has provided good estimates of velocity and attenuation in anisotropic laminates in the frequency range of Lamb wave applications. Comparisons to experimental data and results from literature have been presented in order to validate the model. New shear correction coefficients have been introduced which provide a better matching of the frequencies from the approximate theory to frequencies obtained from the exact theory. However, it was also depicted that the model suffers from some limitations that prevent it from being used to solve the whole spectrum of composite laminate problems, i.e.

high frequency range. It is also well known from literature that higher order theories accuracy deteriorates as the laminate becomes thicker. Nevertheless, dispersion

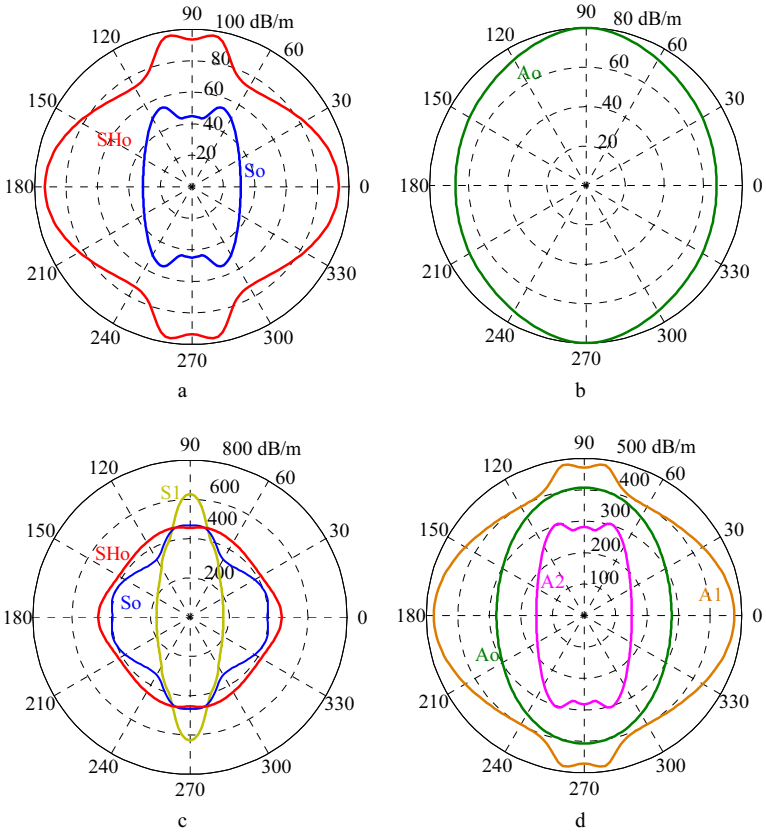

Fig. 6. **Attenuation of Lamb waves: a, b - attenuation polar plot at 100 kHz; c, d - attenuation polar plot at 500 kHz**.

knowledge gained with this fast modelling approach is of great importance for NDT and SHM applications since it plays a critical role in the selection of the optimal inspection frequencies for the improvement of the sensitivity and for optimization of sensor networks in terms of sensor placement and number of sensors.

Acknowledgment

The authors would like to express their gratitude to the Research School on Multi-Modal Sensor Systems for Environmental Exploration (MOSES) and the Center for Sensor Systems (ZESS) for sponsoring the research presented herein. Furthermore, the authors thank Dr.-Ing. Rolf T. Schulte from the University of Siegen, Department of Technical Mechanics, for fruitful discussions concerning the implementation proposed methodology.

Appendix

For the case of symmetric laminates the equations of motion can be decoupled into two independent matrices. In order to obtain solutions for the symmetric and antisymmetric modes of propagation, combinations of frequency and wavenumber where the matrices determinants go to zero must be found. The symmetric modes are governed by

$$L_s x_s = \begin{bmatrix} L_s^{11} & L_s^{12} & L_s^{13} & L_s^{14} & L_s^{15} \\ L_s^{12} & L_s^{22} & L_s^{23} & L_s^{15} & L_s^{25} \\ L_s^{13} & L_s^{23} & L_s^{33} & L_s^{34} & L_s^{35} \\ L_s^{14} & L_s^{15} & L_s^{34} & L_s^{44} & L_s^{45} \\ L_s^{15} & L_s^{25} & L_s^{35} & L_s^{45} & L_s^{55} \end{bmatrix} x_s \qquad \text{(A.1)}$$

where $\boldsymbol{x}_s = \{U_0\ V_0\ \Psi_z\ \Phi_x\ \Phi_y\}$ and the terms of L_s are given by

$$\begin{aligned}
L_s^{11} &= A_{11}k_s^2 + A_{66}k_y^2 + 2A_{16}k_xk_y - \omega^2 I_0 \\
L_s^{12} &= A_{16}k_x^2 + A_{26}k_y^2 + (A_{12} + A_{66})k_xk_y \\
L_s^{13} &= i\kappa_3\left(A_{13}k_x + A_{36}k_y\right) \\
L_s^{14} &= D_{11}k_x^2 + D_{66}k_y^2 + 2D_{16}k_xk_y - \omega^2 I_1 \\
L_s^{15} &= D_{16}k_x^2 + D_{26}k_y^2 + (D_{12} + D_{66})k_xk_y \\
L_s^{22} &= A_{66}k_x^2 + A_{22}k_y^2 + 2A_{26}k_xk_y - \omega^2 I_0 \\
L_s^{23} &= -i\kappa\left(A_{36}k_x + A_{23}k_y\right) \\
L_s^{25} &= D_{66}k_x^2 + D_{22}k_y^2 + 2D_{26}k_xk_y - \omega^2 I_2 \\
L_s^{33} &= -\kappa_4^2 D_{55}k_x^2 - D_{44}\kappa_5^2 k_y^2 - 2\kappa_4\kappa_5 D_{45}k_xk_y - \\
&\quad - \kappa_3^2 A_{33} + \omega^2 I_2 \\
L_s^{34} &= i\left(2\kappa_4^2 D_{55} - \kappa_3 D_{13}\right)k_x + i\left(2\kappa_4\kappa_5 D_{45} - \kappa_3 D_{36}\right)k_y \\
L_s^{35} &= i\left(2\kappa_4\kappa_5 D_{45} - \kappa_3 D_{36}\right)k_x + i\left(2\kappa_5^2 D_{44} - \kappa_3 D_{23}\right)k_y \\
L_s^{44} &H_{11}k_x^2 + H_{66}k_y^2 + 2H_{16}k_xk_y + 4\kappa_4^2 D_{55} - \omega^2 I_4 \\
L_s^{45} &= H_{16}k_x^2 + H_{26}k_y^2 + (H_{12} + H_{66})_{xy} + 4\kappa_4\kappa_5 D_{45} \\
L_s^{55} &= H_{66_x}^{\ 2} + H_{22}k_y^2 + 2H_{26}k_{xy} + 4\kappa_5^2 D_{44} - \omega^2 I_4
\end{aligned} \qquad \text{(A.2)}$$

The antisymmetric modes are governed by

$$L_A x_A = \begin{bmatrix} L_A^{11} & L_A^{12} & L_A^{13} & L_A^{14} & L_A^{15} & L_A^{16} \\ L_A^{12} & L_A^{22} & L_A^{23} & L_A^{24} & L_A^{25} & L_A^{26} \\ L_A^{13} & L_A^{23} & L_A^{33} & L_A^{34} & L_A^{35} & L_A^{36} \\ L_A^{14} & L_A^{24} & L_A^{34} & L_A^{44} & L_A^{45} & L_A^{46} \\ L_A^{15} & L_A^{25} & L_A^{35} & L_A^{45} & L_A^{55} & L_A^{56} \\ L_A^{16} & L_A^{26} & L_A^{36} & L_A^{46} & L_A^{56} & L_A^{66} \end{bmatrix} x_A \quad \text{(A.3)}$$

where $x_A = \{W_0 \ \Psi_x \ \Psi_y \ \Phi_z \ \Lambda_x \ \Lambda_y\}$ and the terms of L_A are given by

$$\begin{aligned}
L_A^{11} &= -\left(\kappa_1^2 A_{55} k_x^2 + \kappa_2^2 A_{44} k_y^2 + 2\kappa_1\kappa_2 A_{45} k_x k_y - \omega^2 I_0\right) \\
L_A^{12} &= i\kappa_1\left(\kappa_1 A_{55} k_x + \kappa_2 A_{45} k_y\right) \\
L_A^{13} &= i\kappa_2\left(\kappa_1 A_{45} k_x + \kappa_2 A_{44} k_y\right) \\
L_A^{14} &= -\begin{pmatrix} \kappa_1\kappa_7 D_{55} k_x^2 + \kappa_2\kappa_8 D_{44} k_y^2 + \\ +\left(\kappa_2\kappa_7 + \kappa_1\kappa_8\right) D_{45} k_x k_y - \omega^2 I_2 \end{pmatrix} \\
L_A^{15} &= 3i\left(\kappa_1\kappa_7 D_{55} k_x + \kappa_2\kappa_7 D_{45} k_y\right) \\
L_A^{16} &= 3i\left(\kappa_1\kappa_8 D_{45} k_x + \kappa_2\kappa_8 D_{44} k_y\right) \\
L_A^{22} &= D_{11} k_x^2 + D_{66} k_y^2 + 2D_{16} k_x k_y + \kappa_1^2 A_{55} - \omega^2 I_2 \\
L_A^{23} &= D_{16} k_x^2 + D_{26} k_y^2 + \left(D_{12} + D_{66}\right) k_x k_y + \kappa_1\kappa_2 A_{45} \\
L_A^{24} &= i\left(\kappa_1\kappa_7 D_{55} k_x + \kappa_1\kappa_8 D_{45} k_y + 2\kappa_6\left(D_{13} k_x + D_{36} k_y\right)\right) \\
L_s^{25} &= H_{11} k_x^2 + H_{66} k_y^2 + 2H_{16} k_x k_y + 3\kappa_1\kappa_7 D_{55} - \omega^2 I_4 \\
L_s^{26} &= H_{16} k_x^2 + H_{26} k_y^2 + \left(H_{12} + H_{66}\right) k_x k_y + 3\kappa_1\kappa_8 D_{45} \\
L_s^{33} &= D_{66} k_x^2 + D_{22} k_y^2 + 2D_{26} k_x k_y + \kappa_2^2 A_{44} - \omega^2 I_2 \\
L_s^{34} &= i\left(\kappa_2\kappa_7 D_{45} k_x + \kappa_2\kappa_8 D_{44} k_y - 2\kappa_6\left(D_{36} k_x + D_{23} k_y\right)\right) \\
L_s^{35} &= H_{16} k_x^2 + H_{26} k_y^2 + \left(H_{12} + H_{66}\right) k_x k_y + 3\kappa_1\kappa_7 D_{45} \\
L_s^{36} &= H_{66} k_x^2 + H_{22} k_y^2 + 2H_{26} k_x k_y + 3\kappa_2\kappa_8 D_{44} - \omega^2 I_4 \\
L_A^{44} &= -\begin{pmatrix} \kappa_7^2 D_{55} k_x^2 + \kappa_8^2 H_{44} k_y^2 + \\ +\left(\kappa_7 + \kappa_8\right) H_{45} k_x k_y + 4\kappa_6^2 D_{33} - \omega^2 I_4 \end{pmatrix} \\
L_s^{45} &= 3i\left(\kappa_7^2 H_{55} k_x + \kappa_7\kappa_8 H_{45} k_y\right) - 2i\kappa_6\left(H_{13} k_x + H_{36} k_y\right) \\
L_s^{46} &= 3i\left(\kappa_7\kappa_8 H_{45} k_x + \kappa_8^2 H_{44} k_y\right) - 2i\kappa_6\left(H_{36} k_x + H_{23} k_y\right) \\
L_A^{55} &= K_{11} k_x^2 + K_{66} k_y^2 + 2K_{16} k_x k_y + 9\kappa_7^2 H_{55} - \omega^2 I_6 \\
L_A^{56} &= K_{16} k_x^2 + K_{66} k_y^2 + \left(K_{12} + K_{66}\right) k_x k_y + 9\kappa_7\kappa_8 H_{45} \\
L_A^{66} &= K_{66} k_x^2 + K_{22} k_y^2 + 2K_{26} k_x k_y + 9\kappa_8^2 H_{44} - \omega^2 I_6
\end{aligned} \quad \text{(A.4)}$$

where $k_x = k\ cos(\theta)$, $k_y = k\ sin(\theta)$ and k is the wavenumber. Additionally,

$$(A_{ij}, D_{ij}, H_{ij}, K_{ij}) = \int_{-h/2}^{h/2} \overline{C}_{ij}(1, z^2, z^4, z^6) dz \quad \text{(A.5)}$$

$$(I_0, I_2, I_4, I_6) = \int_{-h/2}^{h/2} \rho(1, z^2, z^4, z^6) dz \quad \text{(A.6)}$$

where $i, j = 1,...,6$, ρ is the density of the material and h is the thickness of the plate. The shear correction coefficients κ_1 to κ_5 where taken according to [9]. The remaining correction factors were calculated by matching specific frequencies from the approximate theory to frequencies obtained from the exact elasticity theory as follows: $\kappa_6 = \pi/\sqrt{15}$ and $\kappa_7 = \kappa_8 = \pi/\sqrt{17}$. The resulting complex wave number $k = k_{Re} + ik_{Im}$ is used to describe the phase velocity of waves travelling through their real part, k_{Re}, and the amplitude decay through their imaginary part, k_{Im}.

References

1. **Staszewski W., Boller C. and Tomlinson G. R.** Health Monitoring of aerospace structures: Smart sensor technologies and signal Processing. Munich: Wiley. 2004.
2. **Kundu T.** Ultrasonic nondestructive evaluation: Engineering and Biological Material Characterization. 1st ed. London: CRC Press. 2003.
3. **Pavlakovic B., et al.** Disperse: a general purpose program for creating dispersion curves. Review of Progress in QNDE. 1997. 16. P. 185-192.
4. **Bartoli I., et al.** Modeling guided wave propagation for structural monitoring of damped waveguides, in Third European Workshop on Structural Health Monitoring. Granada, Spain. 2006.
5. **Reddy J. N.** Mechanics of laminated composite plates and shells: theory and analysis. 2nd ed. New York: CRC Press. 2004.
6. **Calomfirescu M.** Lamb waves for structural health monitoring in viscoelastic composite materials. PhD Thesis. Faserinstitut Bremen, University of Bremen. 2008.
7. **Reddy J. N.** A refined nonlinear theory of plates with transverse shear deformation. International Journal of Solids and Structures. 1984. 20(9-10). P. 881-896.
8. **Mindlin R. D**. Influence of rotary inertia and shear on flexural motion of isotropic elastic plates. Journal of Applied Mechanics Transactions of the ASME. 1951. 18. P. 31-38.
9. **Whitney J. M. and Sun C. T.** A higher order theory for extensional motion of laminated composites Journal of Sound and Vibration. 1973. 30(1). P. 85-97.
10. **Wang L. and Yuan F. G.** Lamb wave propagation in composite laminates using a higher-order plate theory. Vol. 6531. Bellingham, WA, ETATS-UNIS: Society of Photo-Optical Instrumentation Engineers. 2007.
11. **Moll J., Torres Arredondo M. A., and Fritzen C. P.** Numerical aspects of automatic guided wave based damage localization algorithms in flat anisotropic structures. Submitted for publication to "Smart Structures and Systems".
12. **Deschamps M. and Hosten B.** The effects of viscoelasticity on the reflection and transmission of ultrasonic waves by an orthotropic plate. The Journal of the Acoustical Society of America. 1992. 91(4). P. 2007-2015.
13. **Bartoli I., et al.** Modelling wave propagation in damped waveguides of arbitrary cross-section. Journal of Sound and Vibration. 2006. 295(3-5). P. 685-707.
14. **Neau G.** Lamb waves in anisotropic viscoelastic plates. Study of the wave fronts and attenuation. PhD Thesis. L'Universite de Bordeaux. 2003.

M.- A. Torres-Arredondo, C.-P. Fritzen

Klampaus stangrumo plokštelių teorija Lembo bangų sprendimams greitai modeliuoti taikant neardomuosius bandymus ir struktūrinės būsenos stebėseną

Reziumė

Nukreiptosios ultragarso bangos turi daug naudingų savybių, kurios gali būti pritaikytos neardomiesiems bandymams ir struktūrinės būsenos stebėsenai. Tačiau, norint panaudoti šias bangas defektų stebėsenai, kartu naudoti automatinį duomenų apdorojimą ir analizę, reikia turėti daug informacijos apie šių bangų generavimą ir sklidimą. Todėl išmanyti dispersines charakteristikas labai svarbu, kai nustatomas reikiamas jutiklių skaičius ir padėtis. Šiame darbe pateikiama aukštesniosios eilės plokštelių teorija, leidžianti gauti dispersines charakteristikas pluoštais sutvirtintuose kompozituose. Šis metodas leidžia gauti didesnį skaičiavimo efektyvumą ir yra paprastesnis už tradicinius metodus, ypač žemesniųjų dažnių diapazone, kuriame dažniausiai naudojamos Lembo bangos. Straipsnyje pateikiamas palyginimas su eksperimentiniais duomenimis, be to, aptariami metodo apribojimai.

Submitted 29 04 2011